J. Synchrotron Rad. (1998). **5**, 1010–1012

Polarization analysis in the 3–25 keV range at the ESRF magnetic scattering beamline

A. Stunault,[a]* C. Vettier,[a] F. de Bergevin,[b] N. Bernhoeft,[a] V. Fernandez,[a] S. Langridge,[a] E. Lidström,[a] J. E. Lorenzo-Diaz,[b] D. Wermeille,[a] L. Chabert[a] and R. Chagnon[a]

[a]ESRF, BP 220, F-38043 Grenoble CEDEX, France, and [b]Laboratoire Cristallographie, CNRS, 166X, F-38042 Grenoble CEDEX, France. E-mail: stunault@esrf.fr

(*Received 4 August 1997; accepted 29 January 1998*)

The ESRF magnetic scattering beamline has been optimized for easy tunability of the polarization and energy in the 3–40 keV range. The linear horizontal polarization from the undulator reaches 99.9%, with a flux of $\sim 10^{12}$ photons s^{-1} at the sample. The diffractometer can operate in horizontal and vertical geometries, with an energy or polarization analyser. The capabilities of this beamline in terms of flux, energy tunability and polarization, permitted polarization analysis of resonant magnetic scattering from antiferromagnetic UPd_2Si_2 at both the L_2- and M_4-edges of uranium, to separate the contributions of the 5*f* and 6*d* electrons to the magnetism.

Keywords: beamlines; magnetic scattering; polarization.

1. Introduction

Development of magnetic X-ray scattering methods is largely based on the concomitant development of the experimental methods and theoretical progress. A good example of this 'cross-fertilization' is the discovery of resonant exchange scattering (Gibbs *et al.*, 1988). The interactions of X-rays with magnetization densities (Gibbs, 1992, and references within) have the following properties: (i) they rotate the X-ray polarization, (ii) they show resonant features at absorption edges, (iii) the scattered signal is weak away from resonance. Therefore, magnetic X-ray scattering beamlines must allow tunability of the polarization (linear or circular) and of the energy over a wide range. Further properties may be required, such as a small focused beam for studies of microcrystals. The magnetic scattering beamline ID20 at the ESRF combines all these features. Its versatility also allows other studies, such as high-Q-resolution scattering. We will discuss the main characteristics of the beamline and recent experiments that demonstrate the value of the installation.

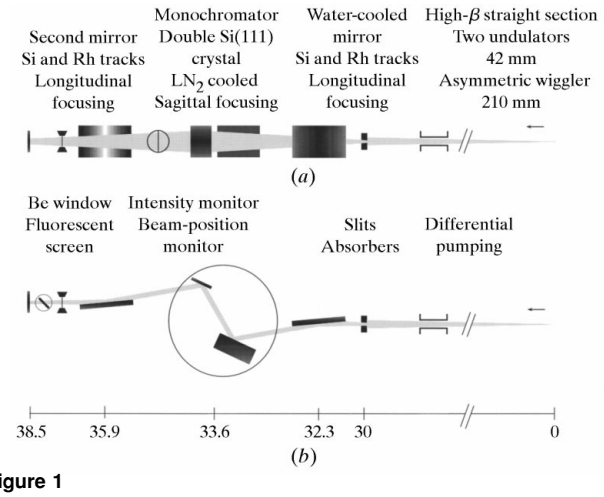

Figure 1
Layout of the optics hutch: (*a*) top view, (*b*) side view.

2. Insertion devices

The energy range of interest for resonant scattering covers the absorption edges of elements that are likely to develop a magnetic moment. Furthermore, if we restrict ourselves to edges whose final state involves a spin-polarized electronic state, the upper limit for the energy can be set to around 40 keV. On the low-energy side, the limit is the Bragg cut-off beyond which no diffraction from crystals is possible: in practice, this is set to 3.0 keV.

The classical way to produce a tunable X-ray polarized beam is to view the electron orbit at different angles. An asymmetric wiggler with a critical energy of 19 keV has been designed and installed in the ID20 straight section. However, new methods based on crystal optics (Giles *et al.*, 1995; Hirano *et al.*, 1991) have been discovered to transform linear polarization into elliptical polarization over a wide energy range. Moreover, wigglers create high heat load on optics elements and do not take advantage of the high brilliance of the ESRF. Therefore, a linear undulator of period 42 mm was mounted around a small-gap vacuum vessel; the undulator gap can be reduced down to 16 mm, which ensures a proper overlap of odd-order harmonics over the whole energy range of interest (3–25 keV). At present, the flux available at the sample ranges from 2×10^{12} photons s^{-1} at 4 keV to 10^{13} photons s^{-1} at 10 keV at 200 mA.

3. Optics hutch

The general layout of the optics is shown in Fig. 1. To ensure a high flux at the sample, the number of windows in the beam has been reduced. The optics system is only separated from the storage-ring vacuum by differential pumping that keeps the pressure in the front end below 5×10^{-9} mbar (Renier & Draperi, 1997). All the optics are under UHV conditions, with a base pressure in the 5×10^{-9} mbar range. With the beam at full power, the pressure rises to 5×10^{-8} mbar before the monochromator.

The beamline optics comprise a double-crystal monochromator with sagittal focusing between two mirrors with variable longitudinal focusing. The full beam from the source can be focused down to 300×200 μm at the sample. The optics system is mounted on a long rigid girder that can be lifted to view the source point from above or below the electron-orbit plane.

The double-crystal assembly of the monochromator is mounted on a rotating spindle with a differential pumping stage. The rotation stage, which is equipped with an incremental encoder, has an accuracy of ±0.6 arcsec and a reproducibility better than ±0.4 arcsec, *i.e.* ±0.1 eV at 9 keV. The crystals are Si(111) single crystals. The (333) reflection is used above 25 keV. The first crystal is cryogenically cooled to minimize the amount of lattice strain under a large heat load. All cryogenics tubes have been optimized to keep the amount of vibration as low as possible. Tunable sagittal focusing is ensured by the 0.7 mm-thick second crystal (rectangular with stiffening longitudinal ribs on the back) mounted on a crystal bender. The parallelism of both crystals is adjusted using piezoelectric translators. Their elongation is

controlled in a closed loop by strain gauges; this ensures a stability of the double-crystal set-up over periods of days.

The mirrors have been designed to reduce the high-order harmonics content and to provide longitudinal focusing over a broad energy range. They are made of 1 m silicon ingots polished by the SESO company and contain two reflecting surfaces: pure silicon and a 600 Å-thick rhodium layer. The two tracks can be exchanged by translating the mirrors perpendicularly to the X-ray beam. Bending is achieved with four independent lever systems; the bending moment is controlled by strain-gauge load cells. Radii of curvature are controlled with X-rays using the pencil-beam method. Curvatures from 0.8 km to 30 km can be achieved with a slope error of ±2 µrad r.m.s. The optical roughness of the surfaces is around 5 Å; measured reflectivity curves at various energies indicate a 40 Å 'short-wavelength' rhodium roughness. Nevertheless, these mirrors have an excellent low-angle reflectivity, reaching 90% for the two mirrors. The first mirror is water-cooled to extract the 500 W heat load up to the highest incident angle (8 mrad).

Two wire beam-position monitors (Fajardo & Ferrer, 1995) probe the stability of the X-ray beam. Retractable intensity monitors are used to tune the slits and monochromator positions.

The optics hutch contains the 500 µm-thick Be window that separates the optics UHV vacuum from the beamline vacuum. A secondary shutter after this window allows the optical components to be kept under heat load even when work is carried out in the experimental hutch, which improves their thermal stability. Under these conditions, the beam position at the sample is stable within ±10 µm over periods of at least 24 h.

4. Experimental hutch

The experimental station contains a long flight path for the monochromatic X-ray beam and a robust diffractometer (Fig. 2). Various X-ray optics items can be inserted into the flight path. The default configuration includes a wire X-ray beam-position monitor and a polarization monitor. Diamond crystals of various thickness can be mounted as phase plates and tuned to provide circular polarization over a wide energy range (6–15 keV).

Figure 2
The '12 circle' diffractometer of ID20.

The diffractometer has been designed for experiments in both the vertical and the horizontal scattering planes in a four-circle geometry with a possible extension to the two-axis configuration in case a heavy and bulky sample environment is required. It was built by the MicroControle-Newport company and great care was taken to minimize the sphere of confusion even in the presence of high mechanical loads: 40 µm in the vertical scattering plane geometry, and 30 µm in the horizontal geometry. A linear polarization analyser can be mounted on each detector arm, as well as a classical crystal analyser set-up. The polarization analyser assembly, based on a crystal scattering at angles close to 90°, can rotate about the X-ray beam scattered by the sample in order to make a full linear-polarization analysis.

5. Polarization dependence of magnetic scattering from UPd_2Si_2

A typical example of the studies made available by this beamline is the antiferromagnetic phase transition in tetragonal UPd_2Si_2. UPd_2Si_2 orders antiferromagnetically below 108 K. Polarization analysis at the M_4-edge of uranium (3.728 keV) is a challenge due to the high absorption. All pathways up to the analyser crystal are evacuated, the beam passing through thin Kapton windows, and the spaces around the analyser crystal and to the detector are pressurized with helium. The efficiency of the whole analyser set-up [Al(111) crystal reflectivity, flight path through helium and an extra Kapton window] reaches 10%, and the detected magnetic intensities were still as high as 20000 photons s^{-1} in the rotated σ–π channel. Such high intensities can easily be used to analyse the electronic origin of the magnetic signals. The scattered intensity has its polarization fully rotated (Fig. 3), which implies that the resonance is of dipolar type and due to 3*d*–5*f* transitions. Polarization analysis at the L_2-edge of uranium (20.948 keV) is technically much easier, but the resonance is weaker and the reflectivity of the used LiF(0 0 10) reflection is only 1% at this energy. The intensities detected in the σ–π channel are small (10 photons s^{-1}), but benefit from the very low background (less than 1 photon s^{-1}) in this channel. The angular dependence of the σ–π resonance and the absence of signal in the σ–σ channel are consistent with a dipolar origin, reflecting the spin polarization of the 6*d* shell.

6. Conclusions

A wide range of X-ray magnetic-scattering studies has been made possible, or at least easier and much less time demanding, by the

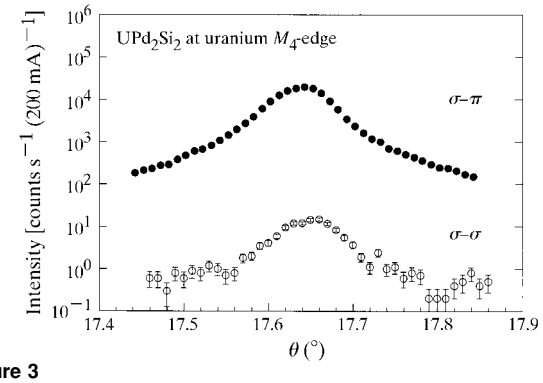

Figure 3
Polarization analysis at the M_4-edge of uranium in UPd_2Si_2. The low count rates measured in the σ–σ channel (open circles) are due to leakage from the intense σ–π channel (full circles).

optimization of the flux and energy resolution at the ESRF magnetic-scattering beamline. Further improvements are also under way, with the installation of two phased undulators, bimorph focusing mirrors and a high-energy-resolution monochromator.

We thank A. Draperi, G. Rostaing, Y. Dabin, G. Marot, C. Giles and A. Andrejczuk for their contributions to the construction of ID20.

References

Fajardo, P. & Ferrer, S. (1995). *Rev. Sci. Instrum.* **66**, 1882–1884.
Gibbs, D. (1992). *Synchrotron Rad. News*, **5**, 18–23.
Gibbs, D., Harshman, D. R., Isaacs, E. D., McWhan, D. B., Mills, D. & Vettier, C. (1988). *Phys. Rev. Lett.* **61**, 1241–1244.
Giles, C., Malgrange, C., Goulon, J., de Bergevin, F., Vettier, C., Fontaine, A., Dartyge, E., Pizzini, S., Baudelet, F. & Freund, A. (1995). *Rev. Sci. Instrum.* **66**, 1549–1553.
Hirano, K., Izumi, K., Ishikawa, T., Annaka, S. & Kikuka, S. (1991). *Jpn. J. Appl. Phys. Lett.* **30**, L407–410.
Renier, M. & Draperi, A. (1997). *Vacuum*, **48**, 405–407.